Benzene Methylation by Methyl Mercaptan over Acidic Chabazite: Concerted or Stepwise Mechanism?

Robin Gaumard, Hazar Guesmi, Patrizia Calaminici, Andreas Köster, Juan Diego Samaniego Rojas, Tzonka Mineva

Benzene methylation by methyl mercaptan over acidic chabazite: concerted or step-wise mechanism?

Robin Gaumard,[†] Hazar Guesmi,[†] Patrizia Calaminici,[‡] Andreas Köster,[‡] Juan Diego Samaniego Rojas,[‡] and Tzonka Mineva[*,†]

[†]*ICGM, Univ Montpellier, CNRS, ENSCM, Montpellier, France*

[‡]*Departamento de Química, CINVESTAV, Av. Instituto Politécnico Nacional 2508, AP 14-740, México D.F. 07000 México*

E-mail: tzonka.mineva@enscm.fr

Abstract

The elimination of methyl mercaptan from natural gas sources and many industrial processes remains an actively investigated issue. The discovery that acidic zeolites are efficient catalysts for the decomposition and conversion of methyl mercaptan to value-added products has prompted the need for better understanding of the fundamental reaction mechanisms. Periodic density functional theory calculations with empirical dispersion corrections were employed in this work to investigate the mechanism of the toluene formation from benzene and methyl mercaptan over acidic chabazite (H-CHA) zeolite. The free energy surfaces (FESs) along the step-wise and the concerted mechanisms of mercaptan and methanol reagents are identified and compared. Although mercaptan is the chemical analog of methanol, we found that mercaptan conversion is possible only along the step-wise route, owing to the larger size of sulfur if co-adsorbed with benzene in the H-CHA zeolite pore. Both reagents undergo their conversion via

the same rate-limiting steps, which are the formation of the surface-bound methoxide (step-wise route) and C-C bond formation from the co-adsorbed CH_3XH (X = S, O) and C_6H_6 molecules (concerted route). The ab-initio molecular dynamics simulations at the reactive temperatures revealed intra-molecular hydrogen transfer in the toluenium cation that facilitates the H-back-donation for the catalyst regeneration.

Introduction

Methyl mercaptan (CH_3SH), a harmful sulfur-containing volatile compound (SVOC), can be efficiently converted into hydrocarbons over acidic H-ZSM zeolite catalysts.[1–4] Other thiols (C1-C3 mercaptans) can also be decomposed on zeolites with acidic Brønsted H-sites.[5,6] Hulea et al.[5] reported high selectivity of H-ZSM-5, H-Y, H-Ferrierite, and H-SAPO-34 catalysts in the conversion of mixtures of ethyl and methyl mercaptan into hydrocarbons and H_2S.[5] Mashkina et al.[6] developed processes for dimethyl disulfide transformation to methane without other reagents over H-ZSM-5, Co-H-ZSM-5, and H-NaY catalysts. More recently, the conversion of methyl mercaptan to value-added products was obtained by Cammarano et al.[4] The authors were able to produce xylene from the methylation of toluene by CH_3SH over H-ZSM-5 catalyst. The transformation of SVOCs over acidic zeolite catalysts is therefore beneficial as it avoids the use of solvents or additional reagents, currently implemented for the mecraptan removal in the industrial processes, and allows the complete decomposition of mercaptan, or other thiols, into hydrocarbons and hydrogen sulphide (H_2S).[1–6] Moreover, the high catalytic activity of H-ZSM-5 in Friedel-Crafts reaction of toluene alkylation by methyl mercaptan to xylene,[4] paves the route for further developments of sustainable processes for thiols conversion into value-added products.

Despite these benefits, the conversion mechanisms of methyl mercaptan to hydrocarbons (M2TH) is still not resolved, different to the conversion process of methanol (the oxygen analog of methyl mercaptan) to hydrocarbons (MTH).[7] Comparison between M2TH and MTH over H-ZSM-5 zeolite catalysts under the same conditions revealed similarities, but also non-

negligible differences regarding the catalyst lifetime and the formation of products.[5] In the M2TH process, CH_4 represents more than 90% of the products, whereas in the MTH process a significant amount of olefins were formed in addition to aromatics BTX (benzene-toluene-xylene) and alkanes.[8–13] In the M2TH process, the olefins are absent.[1,4–6] Furthermore, it is well-known that the methanol and the methyl halides are efficient alkylation agents for aromatics, whereas only one study[4] has hitherto reported on the methylation ability of mercaptan to alkylate toluene. The high alkylation yield, obtained for CH_3SH at 450°C was attributed to the lower consumption of CH_3SH in light hydrocarbons in comparison to toluene alkylation by methanol.[4]

Few theoretical works, using density-functional theory (DFT), have been hitherto devoted to the mechanisms of CH_3SH decomposition over acidic zeolites,[14,15] including our work.[14] The comparison between the reaction pathways of methanol and mercaptan decomposition over H-ZSM-5 without other reagents[14] revealed similar basic reaction mechanisms. Analogous conclusions were drawn from the mechanistic study of CH_3SH and CH_3OH conversion to ethene over acidic chabazite (H-CHA).[15] It can be therefore assumed that also the alkylation of aromatics by mercaptan might follow the same step-wise and concerted reaction mechanisms (see Scheme 1), which have been accepted for methanol reagent in the MTH processes.[8,11,16–20]

In the step-wise mechanism, methanol dehydrates onto a Brønsted acid site of the zeolite leading to the formation of surface-bound methoxide (methoxy) species. Consequently the methoxy species methylate aromatics following the Eley-Rideal-type reaction.[11] In the concerted mechanism, methanol and aromatics are co-adsorbed onto a single acid site and then react in a concerted step. The extensive mechanistic research did not yet lead to a conclusive preference of the methanol alkylation mechanism, being still a matter of debates.[8,16–20] A possible reason for the inconclusive mechanistic research is the complexity of the MTH process involving a large variety of intermediates, active complexes and products that may depend on the zeolite topology, the local structures and density of the acid sites. Despite

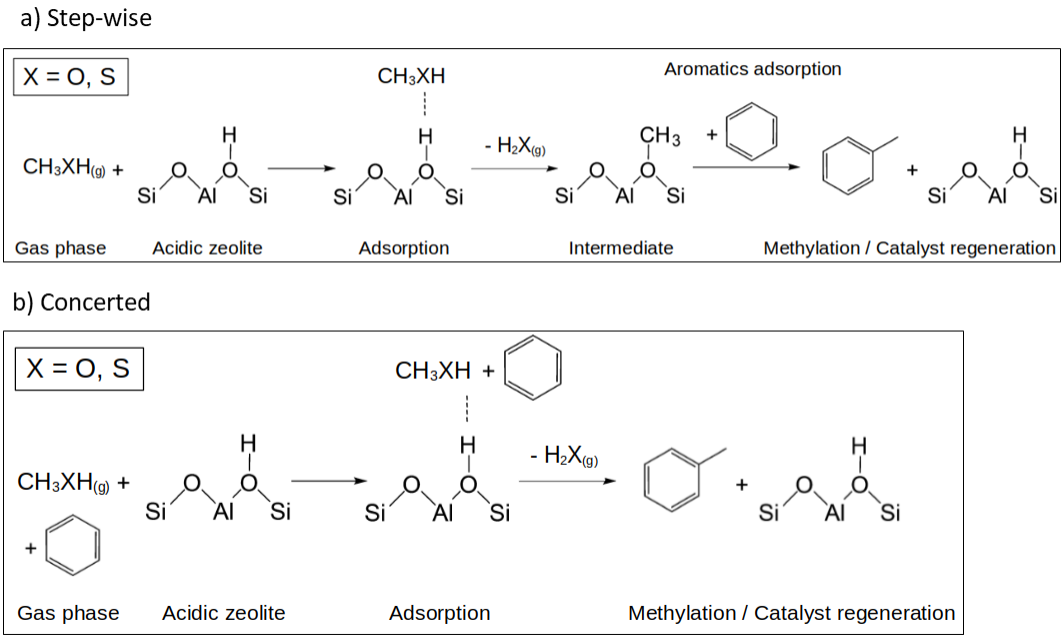

Scheme 1: Schematic presentation of a) the step-wise and b) the concerted mechanism

the complexity of MTH processes, the involvement of surface methoxide species has been confirmed by various spectroscopic and kinetic studies as a key reactive intermediate in methanol conversion and methylation processes by methanol over zeolite catalysts.[21–30]

In this theoretical work we address the question of the reaction mechanisms of benzene methylation by methyl mercaptan over H-CHA zeolite by comparing the free energy surfaces (FES) of the reaction along the step-wise and the concerted pathways. A comparison with methanol reagent over the same zeolite model is also provided. The methylation of benzene by methanol is another well-known technologically important process that offers the production of chemical precursors, such as ethylbenzene, diethylbenzene, toluene and xylenes for production of many fine chemicals.[31] Zeolites with CHA topologies (SAPO-34 and SSZ-13) have been established to be among the best performing catalysts for methanol transformation to aromatic polymethylbenzenes and their corresponding carbenium ions as valuable intermediates in the production of olefins.[32–34] Mercaptan might be an alternative to methanol for benzene methylation that would enable the transformation of harmful mercaptan into

value-added chemicals. The mechanistic studies reported in this work, obtained with a periodic DFT-D3 approach, demonstrated that methyl mercaptan can methylate benzene on a model H-CHA catalyst as efficiently as methanol in the step-wise reaction process.

Methods and Computational Details

DFT Computational Details

A periodic DFT-based approach was used to carry out a full geometrical optimization (atomic positions and unit-cell parameters) and numerical frequency calculations of the minima and maxima states along the reaction paths (step-wise and concerted routes), using the Crystal17 program, based on atom-centered Gaussian orbitals.[35] The stationary points on the potential energy surfaces (PES) that correspond to adsorbates (A), intermediates (I) and activated complexes (transition state complexes, TS) were searched by geometry optimization algorithms. For the location of the minimum energy structures, we performed analytic geometry optimization of the atomic coordinates and cell parameters with the Broyden–Fletcher–Goldfarb–Shanno (BFGS) Hessian update algorithm.[36] The maximum energy structures were located using the distinguished reaction coordinate algorithm[37] with Schlegel Hessian update Model 2.[38] The minimum energy states were confirmed by the absence of imaginary frequencies and the maximum energy structure by the presence of one imaginary frequency. The imaginary frequency values for the transition state structure, located along the step-wise and concerted pathways are reported in Tables S1 and S2, respectively, in the Supplementary Information (SI) section. The convergence criteria for the root mean square gradients and coordinates displacements were set to 10^{-3} a.u., and the convergence criterion for the total electronic energy was everywhere set to 10^{-10} a.u..A shrinking factor of 3×3 was used to generate the commensurate k-points grid in the reciprocal space within the Monkhorst-Pack method.[39] Increasing the shrinking factor up to 4x4 and 6x6 did not lead to different adsorbate and transition state structures, or energies. The vibrational frequencies

were computed at the Γ point[40,41]

All-electron basis functions of triple ζ (pob-TZVP) quality were used for all the atoms (H, C, O, Al, Si and S).[42] A comparison between PES, obtained with double-ζ (pob-DZVP) bases of the conversion of CH_3SH and CH_3OH to methoxy intermediate is presented in Figures S1 and S2, respectively. As follows, the pob-DZVP and pob-TZVP energy profiles show the same trends, however the pob-DZVP bases produced larger ΔE_{ads} and smaller ΔE_{TS} values. Moreover, bases of double ζ quality may produce larger basis set super position errors (BSSE) when applied to zeolites in combination with hybrid DFT functionals.[43] Other problem of using pob-DZVP bases is the larger numerical errors in the vibrational frequency calculations, leading to an increased number of spurious imaginary frequencies in comparison with the pob-TZVP results, as reported in Tables S1 and S3. Therefore, we have chosen triple ζ bases for the present study. Three approximations for the exchange-correlation functionals were tested: the generalised gradient-corrected PBE,[44,45] the hybrid B3LYP[46,47] and the meta-generalised gradient-corrected M06[48] approximations. The benchmark results were carried out again for the step-wise mechanism and are presented in Figs. S3 and S4, and in Table S4 of the SI section. The difference between the three functionals is not significant for the final conclusions and therefore the results, presented in the main text, are those obtained with the PBE approximation. The empirical London dispersion (D3) term with the Becke-Johnson damping function[49–51] was included in all the calculations.

The Gibbs free energy $G^{(i)}(T)$ of each state, labeled as i, of the FESs is computed using the following relation:

$$G^{(i)}(T) = E_L^{(i)} + E_{ZPE}^{(i)} + E_T^{(i)}(T) + (PV)^{(i)} - TS^{(i)}(T) \quad (1)$$

where $E_L^{(i)}$, $E_{ZPE}^{(i)}$, $E_T^{(i)}$(T), denote, respectively, the electronic energy, the zero-point corrected energy, and the thermal contribution to the vibrational energy, and P, V, T, and $S(T)$ denote, respectively, the pressure, the volume, the temperature, and the entropy.

The electronic energies of the zeolite − molecule(s) complexes are corrected for BSSE. The counter-poise approach was used to compute the BSSE corrections by considering the optimized geometries of the reagents in the zeolite − molecule(s) complexes according to the following equations.

$$E_L^{(i)(CP)} = E_L^{(i)} - E_{L,BSSE}^{(M_i)} - E_{L,BSSE}^{(Z_i)} \tag{2}$$

$$E_{L,BSSE}^{(M_i)} = E_L^{(M_i)(C_i-basis)} - E_L^{(M_i)(M_i-basis)} \tag{3}$$

$$E_{L,BSSE}^{(Z)} = E_L^{(Z_i)(C_i-basis)} - E_L^{(Z_i)(Z_i-basis)} \tag{4}$$

In the above equations Z_i and M_i label, respectively, the zeolite (H-CHA or CH_3-CHA) and the molecule(s) in each complex (C_i), and Z_i-basis, M_i-basis, and C_i-basis denote, respectively, the basis set of the zeolite, molecule(s), and molecule(s)-zeolite complex.

The entropy $S(T)$ and the thermal contribution to the vibrational energy $E_T(T)$ were computed from the vibrational frequencies according to the double harmonic approximation using the following formula implemented in the Crystal17 program:[35]

$$S(T) = k_B \sum_j \left[\frac{\hbar\omega_j}{k_B T \left(e^{\frac{\hbar\omega_j}{k_B T}} - 1 \right)} - \log\left(1 - e^{-\frac{\hbar\omega_j}{k_B T}} \right) \right] \tag{5}$$

$$E_T(T) = \sum_j \hbar\omega_j \left[\frac{1}{2} + \frac{1}{e^{\frac{\hbar\omega_j}{k_B T}} - 1} \right] \tag{6}$$

where $\hbar$ represents the reduced Planck constant, $\omega_j = 2\pi\nu_j$ the circular frequency of the vibrational mode ν_j and k_B the Boltzmann constant. The pressure P was taken as $P =$ 1 bar and the volume V of the system was taken as the product of the optimised cell parameters in $Å^3$. These formulas are defined only for positive vibrational modes ($\nu_j > 0$ cm^{-1}). We have corrected the entropy (5) and the thermal contributions (6) for few spurious negative frequencies (< 100 cm^{-1}) due to the imprecision of the numerical calculations of the vibrational modes,[52] by setting the small negative frequencies equal to 10 cm^{-1} and adding

them into eq. (5) and eq. (6). These corrections for one spurious imaginary frequency amount to -2.23 kcal/mol (T = 673 K) and -2.87 kcal/mol (T = 823 K).

The Gibbs free energies of adsorption $\Delta G_{ads}(T)$, of transition state $\Delta G_{TS}(T)$, of formation $\Delta G_F(T)$ and of desorption $\Delta G_{des}(T)$ were computed using the following relations:

$$\Delta G_{ads}(T) = G_{ads}(T) - [G_{CH_3XH}(T) + G_{H-CHA}(T)] \tag{7}$$

$$\Delta G_{TS}(T) = G_{TS}(T) - G_{ads}(T) \tag{8}$$

$$\Delta G_F(T) = G_I(T) - G_{ads}(T) \tag{9}$$

$$\Delta G_{des}(T) = G_{des}(T) - G_I(T) \tag{10}$$

where $G_{ads}(T)$, $G_{CH_3XH}(T)$, $G_{H-CHA}(T)$, $G_{TS}(T)$, $G_I(T)$, $G_{des}(T)$ denote the Gibbs free energy, respectively, of the adsorbate state, the reagents (CH_3XH and H-CHA), the transition state, the intermediate state, and the desorbate state. The sum $G_{CH_3XH}(T)+G_{H-CHA}(T)+G_{C_6H_6}(T)$ is taken as a reference and corresponds to the point 0 of the FESs (see below).

BOMD Computational Details

Born-Oppenheimer Molecular Dynamics (BOMD) simulations were carried out in order to qualitatively examine the short-time stability (and evolution) of the structures at the stationary points on PES at T = 673 and 823 K, that correspond, respectively, to the experimental reaction temperature of the conversion of methanol and methyl mercaptan.[5] We used the open-source code Quantum Espresso[53,54] based on plane waves and pseudopotentials.[55,56] The wave-function and charge density energy cut-offs were set to 60 Ry and 720 Ry, respectively. The PBE functional and ultra-soft-pseudo-potentials[56] were used in the electronic structure calculations. D3 type of correction for the London dispersion was added. We used the Berendsen thermostat[57,58] for rescaling the atomic velocities during the dynamics. The selected thermostat ensures rapid thermalization to the reaction temperature, preventing

high instantaneous temperatures that might cause unphysical structural distortions in the zeolite. In this algorithm, the classical equation of Newton applied to the nuclei is modified according to the following relationship:

$$m_i \dot{\mathbf{v}}_i = \mathbf{F}_i + m_i \gamma \left(\frac{T_0}{T} - 1 \right) \mathbf{v}_i \tag{11}$$

where m_i is the mass of the nucleus i, $\mathbf{F}_i$ is the force applied to each nuclei, $\mathbf{v}_i$ and $\dot{\mathbf{v}}_i$ are, respectively, the velocity and acceleration, T_0 is the target temperature of the thermostat, T is the temperature of the system, and γ is the damping constant, which represents the strength of the coupling. At each time step Δt of the dynamics, the atomic velocities are rescaled proportionally with the parameter λ according to the change in the temperature. The new atomic velocities then become $\mathbf{v}_i = \lambda \mathbf{v}_i$ and the relation of the parameter λ reads

$$\lambda = \sqrt{1 + \frac{\Delta t}{\tau_T} \left(\frac{T_0}{T} - 1 \right)} \tag{12}$$

where τ_T corresponds to the time constant of the coupling. The time constant τ_T was set to $4\Delta t$ for all the calculations. The Velocity-Verlet[59,60] algorithm was used for integrating the equations of motion at each iteration and the default integration step $\Delta t = 0.96$ fs in the Quantum Espresso software was used. The energy convergence threshold was set to 10^{-7}a.u.. The atomic velocities were taken initially as a random thermalised distribution for all the dynamic simmulations. The simulation length of each state amounts to 20 ps. The target temperature for all the structures was reached within less than 1 ps as illustrated in Fig. S5, where the temperature evolution as a function of the simulation time is plotted for a representative case.

Chabazite Model

The DFT calculations and BOMD were carried out on a periodic CHA model, depicted in Fig. 1, and taken from the theoretical work of Sierka and Sauer[61] on proton mobility in acidic chabazite. The unit-cell of the acidic chabazite (H-CHA) contains 37 atoms. In this study we considered only one acidic site in the zeolite, that corresponds to a Si/Al ratio of 11. According to the International Zeolites Association (IZA) structure database,[62] CHA is a material with rhombohedral unit cell and belongs to the $R\bar{3}m$ symmetry group. It is built of two composite units called *d6r* and *cha* units.

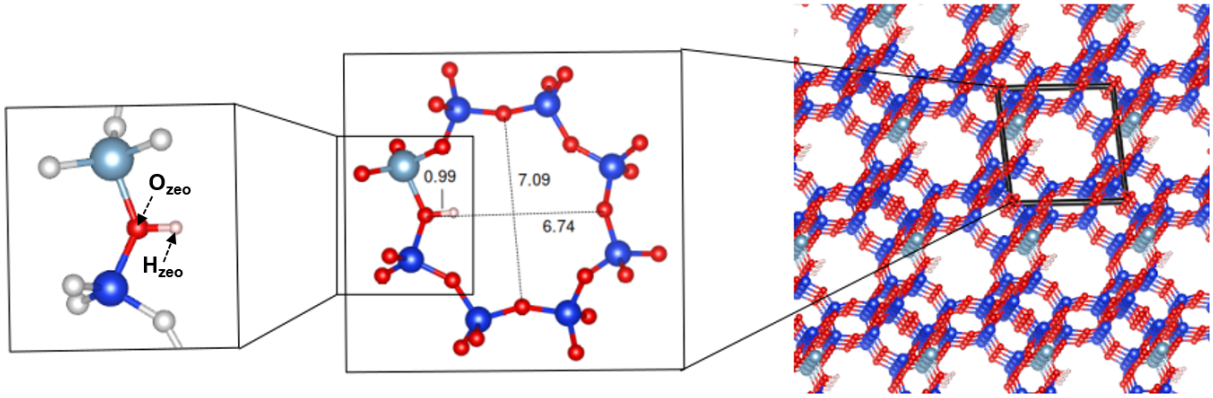

Figure 1: Representation at different levels of the crystalline structure of H-CHA (left: Brønsted acid site, middle: 8-MR ring dimensions in Å, right: periodic structure of H-CHA).

The largest 8 member rings (8-MR) of the CHA topology can include a sphere with a maximum diameter of 7.37 Å that is slightly larger (by 1 Å) than the 10 MR in ZSM-5 zeolite,[62] hitherto pointed out to be the most active catalyst in the conversion of methyl mercaptan to hydrocarbons.[5] The optimized cell parameters and atomic positions of the H-CHA crystal as obtained with the PBE functional are: $a = 9.558$ Å, $b = 9.513$ Å, $c = 9.490$ Å, $\alpha = 94.5°$, $\beta = 94.6°$ and $\gamma = 96.7°$. These values are close to the cell parameters of pure chabazite CHA reported in the IZA structure database[62] : $a = b = c = 9.420$ Å and $\alpha = \beta = \gamma = 94.47°$.[63] This reveals that the presence of one acidic site in the chabazite does not have a large influence on the chabazite structure. All T-positions in CHA are symmetry

equivalent, which makes it an appealing structure to use in theoretical study of acidic site reactivity, independently on the Al-position in the 8-MR ring.

Results and discussion

The production of xylene from toluene methylation by methanol and mercaptan was the main reaction observed in the temperature range of 623 - 823 K over H-ZSM-5 catalyst.[4] The typical temperature regime for the conversion of methyl mercaptan to hydrocarbons over acid zeolites is between 673 and 823 K,[1,6,9] whereas methanol converts in the 523 - 723 K temperature interval. We have, therefore, chosen to compute the entropies and the thermal corrections to the Gibbs free energies (eqs. 5 and 6) at T = 673 and 823 K.

Step-wise mechanism

The zero-point corrected energies (T = 0 K) and ΔG at T = 673 and 823 K of adsorption, activation, formation of intermediates, and product desorption processes (computed from eqs. 7 - 10) are collected in Table 1. The relative Gibbs free energies at T=673 K are plotted in Fig. 2. The zero reference is set to the sum of the total Gibbs energies of all the involved reagents: H-CHA, two molecules of mercaptan and methanol in gas-phase (g), respectively, and one benzene molecule in gas-phase. The step-wise mechanism involves three main reactions: (i) the adsorption of CH_3XH, (X = S, O) on a Brønsted proton site (A1, A'1 in Fig 2); (ii) the dehydration of methanol/mercaptan via an activation complex TS1 (TS'1) (Fig. 2) to form surface-bound methoxy species (-OCH_3)(I1, I'1 in Fig. 2), and (iii) the interaction of the methoxy intermediate with benzene molecule to form a methylated benzene, which then desorbs from the zeolite surface (see Scheme 1). The reactivity of methanol and methyl mercaptan as methylating agents is therefore comparable only in the first two steps (i) and (ii).

The comparison between the reaction pathways of CH_3SH and CH_3OH to the formation

of -OCH_3 intermediate (I1, I'1 in Fig. 2) reveals a TS1 and TS'1 energy barriers of ∼50 kcal/mol for the conversion of CH_3SH and CH_3OH. This is generally in line with previous PBE-plane wave results, reporting ∼ 50 kcal/mol energy barrier for the CH_3SH conversion to -OCH_3 in H-CHA, being higher by ∼ 5-6 kcal/mol of the energy barrier for methanol tranformation to methoxy intermediate.[15]

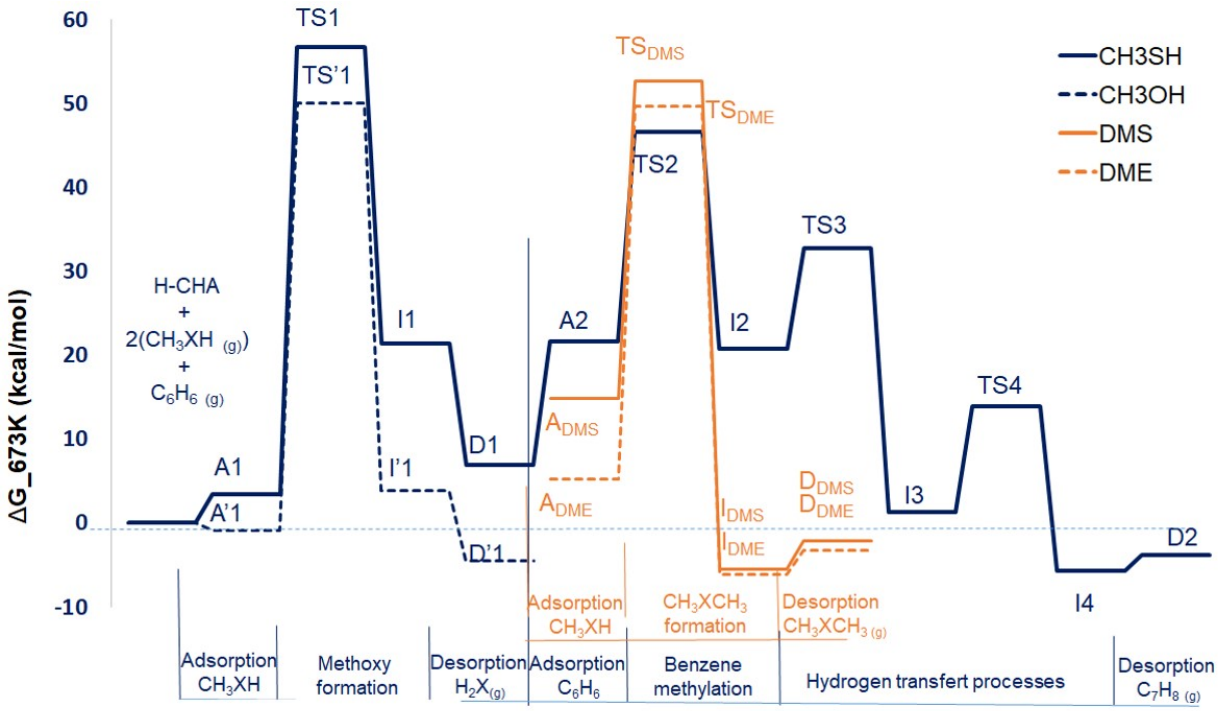

Figure 2: BSSE corrected free energy (ΔG) surface of the step-wise mechanism of the methanol (solid line) and methyl mercaptan (dashed line) methylation of benzene over H-CHA at T = 673 K. The orange solid and dashed lines represent FES of dimethyleter and dymethylsulfide formation (see text), respectively. The zero reference energy is taken as the sum of the gaseous reactant CH_3XH (X = O, S) and C_6H_6, and the solid H-CHA zeolite. The geometries of the stationary states are depicted in Fig. 3

Both reagents adsorb at the Brønsted site of H-CHA zeolite with methanol adsorbing strongly by 4 kcal/mol (see Table 1), similarly to the relative adsorption strengths of both reagents in H-CHA[15] and H-ZSM-5 catalyst.[14] The inclusion of the entropy and the thermal corrections, computed from the harmonic vibrational frequencies, have little to negligible

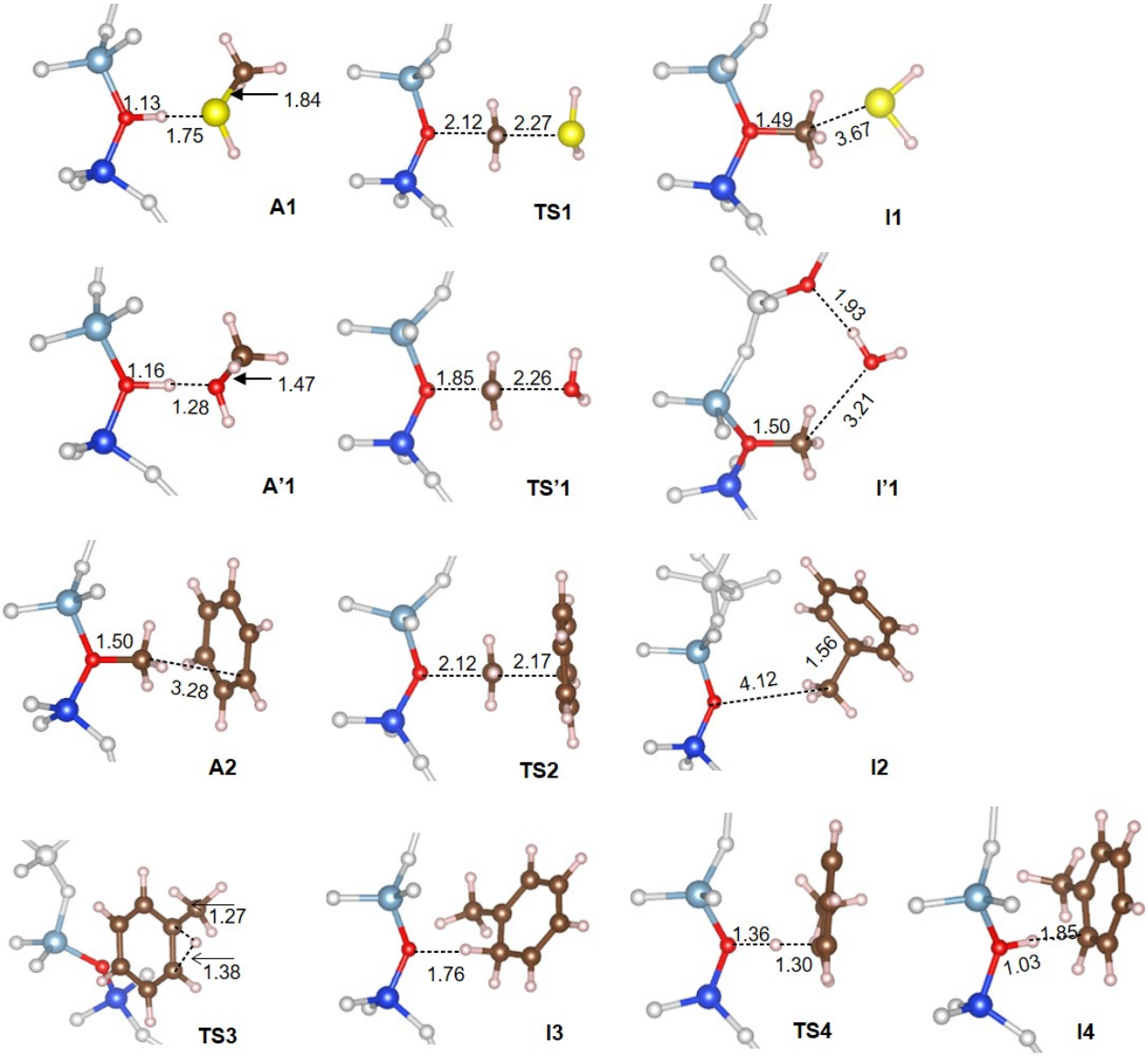

Figure 3: Key geometrical parameters and structures of the adsorbates (A1, A'1, and A2); transition states (TS1, TS'1, TS2, TS3 and TS4), and intermediates (I1, I'1, I2, I3 and I4), located along FES of the step-wise mechanism in the benzene methylation by mercaptan and methanol (structures with primed notations). The distances are given in Å and the color code used for the atoms is the following: Si: dark blue, Al: light blue, O: red, C: brown, S: yellow, H: pink. The atoms coloured in light grey correspond to the atoms of the zeolite.

effect on the energy barriers ΔE_{TS} at T = 0 K as follows from their comparison with ΔG_{TS} at T = 673 and 823 K in Table 1. The entropy and thermal corrections, however, weaken significantly the adsorption energies as already pointed out previously.[14,15] The adsorption energies are also the most sensitive to the BSSE corrections, whereas the transition state

energies, change by a maximum of ∼4-5 kcal/mol as follows from the comparison with the uncorrected for BSSE energies, reported in Table S4.

Table 1: BSSE corrected zero-point energies (T = 0 K) and Gibbs free energies at T = 673 and 823 K along FESs of benzene methylation with CH_3SH and CH_3OH (primed notations). A1 (A'1) and A2 label the adsorbate states of methyl mercaptan (methanol) over H-CHA and of benzene over CH_3-CHA, respectively. TS1 (TS'1), TS2, TS3, TS4 are the transition states in Fig. 2. The intermediate and desorbate states are labelled as follows: methoxy intermediates (I1, I'1), toluenium cations (I2, I3), toluene (I4), H_2X (X = O, S) desorption (D1, D'1) and toluene desorption (D2). The indexes DMS/DME label the states along FESs of DMS/DME formation. All values are in kcal/mol.

CH_3XH + H-CHA → CH_3-CHA + H_2X								
T (K)	A1 (A'1)		TS1 (TS'1)		I1 (I'1)		D1 (D'1)	
0	-23.4 (-27.6)		47.0 (47.6)		21.5 (13.2)		6.6 (7.4)	
673	3.5 (-0.8)		51.0 (50.9)		17.9 (4.7)		-14.5 (-8.3)	
823	9.2 (5.0)		51.9 (51.5)		16.9 (2.3)		-18.8 (-11.5)	
CH_3-CHA + C_6H_6 → H-CHA + C_7H_8								
T (K)	A2	TS2	I2	TS3	I3	TS4	I4	D2
0	-15.3	20.9	-1.4	8.5	-20.4	7.6	-24.2	27.5
673	14.7	24.9	-0.8	11.9	-22.6	14.8	-27.3	1.8
823	21.0	25.8	-0.7	12.6	-23.0	16.4	-28.1	-3.31
CH_3-CHA + CH_3XH → H-CHA + CH_3-X-CH_3								
T (K)	A_{DMS} (A_{DME})		TS_{DMS} (TS_{DME})		I_{DMS} (I_{DME})		D_{DMS} (D_{DME})	
0	-14.6 (-11.4)		27.8 (33.1)		-24.4 (-16.1)		31.2 (29.3)	
673	7.9 (9.7)		35.7 (42.3)		-20.3 (-11.3)		3.4 (2.9)	
823	12.4 (14.0)		37.7 (44.7)		-19.2 (-10.0)		-2.5 (2.7)	

In the step-wise mechanism, the methoxy intermediate methylates benzene after its adsorption in the zeolite pores. The shapes of benzene adsorbate (structure A2 in Fig. 3) and activation complex (structure TS2 in Fig. 3, Fig. S6) closely resemble those reported for benzene methylation in other zeolites, such as H-ZSM-5, H-ZSM-11 and H-β zeolites, obtained in previous DFT (PBE-D3) calculations. In the TS2 complex CH_3 is co-planar to C_6H_6. The methyl carbon aligns with the center of the benzene ring as illustrated in the Fig. S6. The adsorbed benzene (A2) in the CH_3-CHA 8MR pore is rather along the channel, similarly to its orientation in the TS2 and I2 (toluenium ion) configurations.[64,65] The formation of C-C bond is an endothermic reaction with ΔG_{TS} = 24.9 kcal/mol at T=673 K (see Table 1), which is nearly half of the energy barriers TS1 and TS'1 to methoxy formation

from mercaptan or methanol, respectively. This is in line with the mechanistic DFT results of benzene methylation by methanol along the step-wise mechanism.[64–66] Other mechanistic theoretical studies of benzene methylation by mercaptan have not been hitherto conducted, to the best of our knowledge.

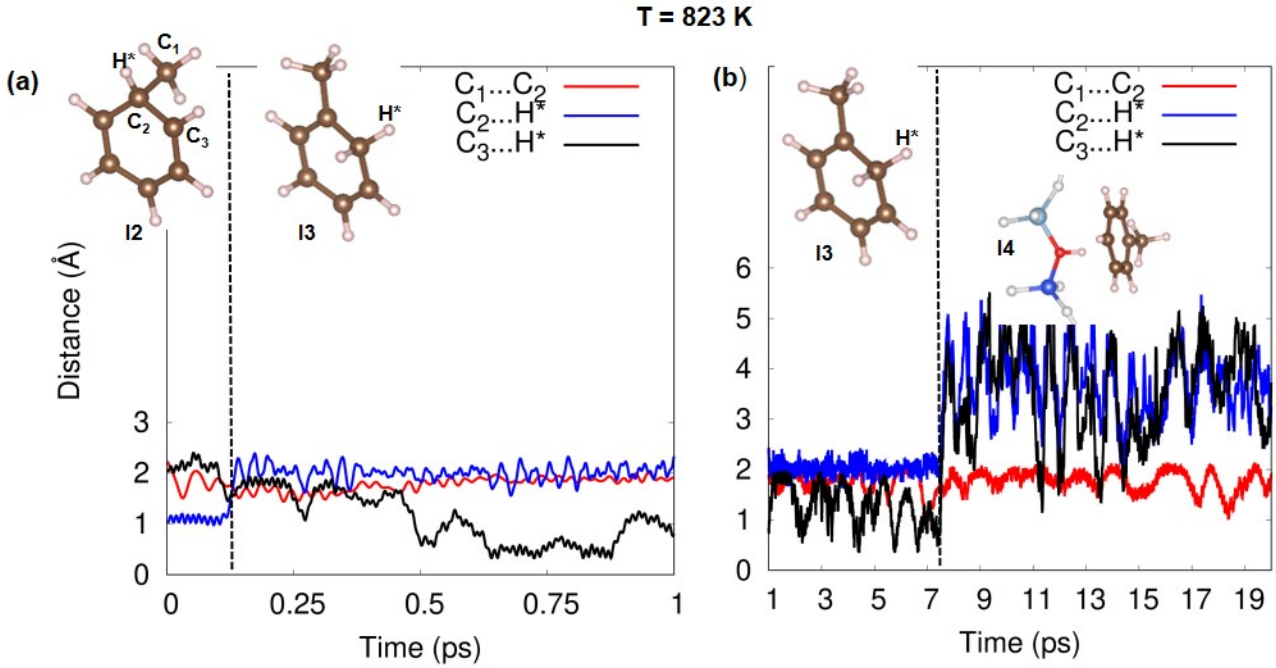

Figure 4: Time evolution of selected C-C and C-H distances in toluenium ion at T = 823 K showing (a) the H* intramolecular transfer and (b) the deprotonation of $C_7H_9^+$. The color code used for the atoms is: Si: dark blue, Al: light blue, O: red, C: brown, H: light pink. Dashed vertical lines correspond to the time instant, at which the H*-transfer occurs from C_2 to C_3 ring carbons (a) and from toluenium ion to the zeolite (b).

After the formation of the toluenium ion I2 at T = 823 K an intramolecular H-transfer between ring carbons in $C_7H_9^+$ was observed along the dynamics simulations after 0.18 ps, followed by the hydrogen back-donation to the zeolite. These H-transfer processes are illustrated in Fig. 4 where the transferred hydrogen of interest is labelled as H*. The subsequent transition state search of the intramolecular H-transfer reaction yielded an energy barrier ΔG_{TS} (TS3 in Fig. 2) of 11.9 and 12.6 kcal/mol at T = 673 and 823 K, respectively, between the intermediates I2 and I3 in Fig2. The H back-donation to regenerate the catalyst (structure I4 in Fig. 3) overcomes the TS4 energy barrier of $\sim$ 15 kcal/mol. An intramolec-

ular H-transfer in $C_7H_9^+$ was not considered in the previous mechanistic studies of benzene methylation by methanol. Instead, it is commonly accepted[8] that $C_7H_9^+$ overcomes rotational barriers[67] around the C2-molecular axis in order to displace in a proper geometry, allowing a direct H back-donation to O_{zeo}. The dynamics simulations at the reactive temperature of mercaptan conversion (823 K), however, evidenced the intramolecular H-transfer as a preferred route for the hydrogen back-donation.

Methoxy-intermediate to dimethysulfide (DMS) and dimethylether (DME)

The DMS and DME products are typically formed below the temperatures at which the transformation of methanol and mercaptan occurs.[4,68,69] Nevertheless, we found it of interest to evaluate the energy barriers for DME/DMS formation and compare them with the barriers of benzene methylation in order to establish whether the benzene methylation in the step-wise route would concur with the DMS/DME production. Only the dissociative (step-wise) mechanism to CH_3-X-CH_3 over CH_3-CHA is considered here, because it is the preferred reaction mechanism at T > 570 K and pressure of 1 bar.[69] The enthalpies and free energies are reported in Table 1 and their structures with the characteristic geometrical parameters of the minima and activation complexes are depicted in Supplementary Fig. S7.

We first note that the energy barriers of the CH_3XH conversions to the methoxy intermediate are significantly higher than ΔG_{TS} to DME/DMS, which indicates the formation of the surface methoxy species as the rate- limitting step. The reactions of methanol and methyl mercaptan reagents follow again the same trend, which is depicted in Fig. 2, with nearly equal ΔG_{ads} ((see Table 1, but different energy barriers. The methylation of CH_3OH by the surface methoxy proceeds with an energy barrier of 42.3 kcal/mol at T = 673 K and of 44.7 kcal/mol at T = 823 K, being higher by ∼6 kcal/mol than ΔG_{TS} in the reaction of CH_3SH to DMS formation. The transition state complexes TS_{DMS} and TS_{DME} at the three temperatures (0, 673 and 823 K) are higher in energy than the TS2 state to the formation of the tolouenium ion (see Table 1). The entropy and thermal corrections at the reaction

temperatures raise ΔG_{TS} of TS_{DMS} and TS_{DME} by ∼8 kcal/mol. The benzene methylation by mercaptane proceeds therefore with lower energy barrier than the formation of DMS species.

Concerted mechanism

According to the concerted (also known as direct) route, the methylation reaction proceeds first with a co-adsorption of CH_3XH (X = O, S) and benzene molecule on the zeolite pore, followed by an interaction of the methyl group in CH_3XH with the benzene molecule in the mobile phase that finally leads to the formation of toluene and H_2X molecule. The free energies of the states along the reaction coordinates are depicted in Fig.5 and their characteristic geometrical structures are presented in Fig. 6. In this mechanism, the surface-bound methoxy species are not formed and the C-C bond is directly created between the methyl group in CH_3XH and benzene. The proton transfer from toluene to the CHA catalyst is mediated now by the H_2X molecule.

Table 2: BSSE corrected zero-point energies (T = 0 K) and Gibbs free energies at T = 673 and 823 K of adsorption (A1_C and A'1_C), transition states (TS1_C, TS1'_C, TS2_C, TS2'_C, TS3_C, TS3'_C), formation (I1_C, I'1_C, I2_C, I'2_C, I3_C and I'3_C) and desorption (D1_C and D'1_C) of toluene and H_2X (X = O, S). All values are in kcal/mol.

$CH_3XH + C_6H_6 + \text{H-CHA} \rightarrow \text{H-CHA} + C_7H_8 + H_2X$								
T (K)	A1_C (A'1_C)	TS1_C (TS'1_C)	I1_C (I'1_C)	TS2_C (TS'2_C)	I2_C (I'2_C)	TS3_C (TS'3_C)	I3_C (I'3_C)	D1_C (D'1_C)
0	-52.1 (-57.8)	85.7 (50.6)	23.6 (18.0)	20.4 (17.1)	6.5 (2.1)	32.4 (21.0)	3.1 (-12.4)	41.7 (51.2)
673	-1.4 (-3.8)	100.3 (55.6)	27.3 (19.5)	26.9 (17.2)	0.8 (-2.4)	45.2 (32.3)	11.6 (-9.4)	-14.1 (-2.2)
823	9.2 (7.8)	104.22 (56.7)	28.1 (19.7)	28.8 (17.4)	-0.7 (-3.8)	48.5 (35.3)	13.6 (-8.6)	-25.9 (-13.8)

We first note that the BSSE corrected ΔG_{ads} of the co-adsorbed CH_3XH and benzene in H-CHA are again very similar, however the co-adsorption of CH_3OH and C_6H_6 after the BSSE and thermal corrections is obtained weaker than the computed ΔG_{ads} at the

same temperature in H-ZSM-5 and H-β zeolites.[64] Our results showed significant dispersion contributions into ΔE_{ads} at T= 0 K, amounting to -40.3 kcal/mol in the co-adsorption of CH_3SH + C_6H_6 and -38.1 kcal/mol in the co-adsorption of CH_3OH + C_6H_6. This points to a strong confinement effect (as computed with D3 dispersion correction) that enhances the co-adsorption of the reagents in H-CHA pore. At T= 0K, i.e. without the contributions of the entropy and thermal contributions, the adsorption energies are -52.1 kcal/mol (CH_3SH) and -57.8 kcal/mol (CH_3OH) and decrease down to -1.4 kcal/mol (CH_3SH) and -3.8 kcal/mol (CH_3OH) at T=673 K.

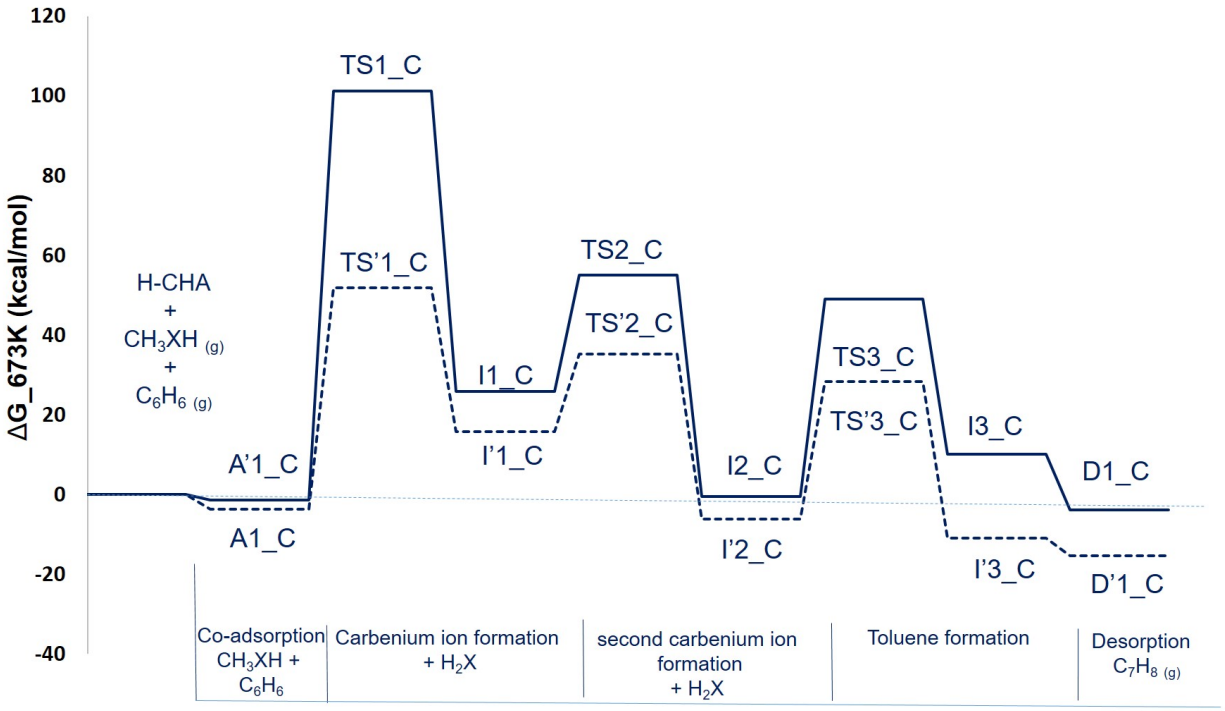

Figure 5: BSSE corrected free energy (ΔG) surface of the concerted benzene methylation mechanism over H-CHA catalyst at T = 673 K for methanol (dashed line) and methyl mercaptan (solid line) as reactant. The prime symbols denote the states involving the CH_3OH reagent. The reference energy (0) is taken as the sum of benzene and CH_3XH in gas phase, and H-CHA in solid phase. A1_C denotes the co-adsorbed reagents, TS1_C, TS2_C and TS3_C label, respectively, the transition state to form the C-C bond in a toluenium ion intermediate (I1_C), the toluenium intramolecular H-transfer to the intermediate I2_C, and the H-transfer between toluenium ion and H_2X mediating the H back-donation to the zeolite (I3_C). D1_C is the desorption of the products (toluene + H_2X) in gaseous phase.

As follows from Fig. 5, the C-C bond formation is the rate-limiting step, in line with all

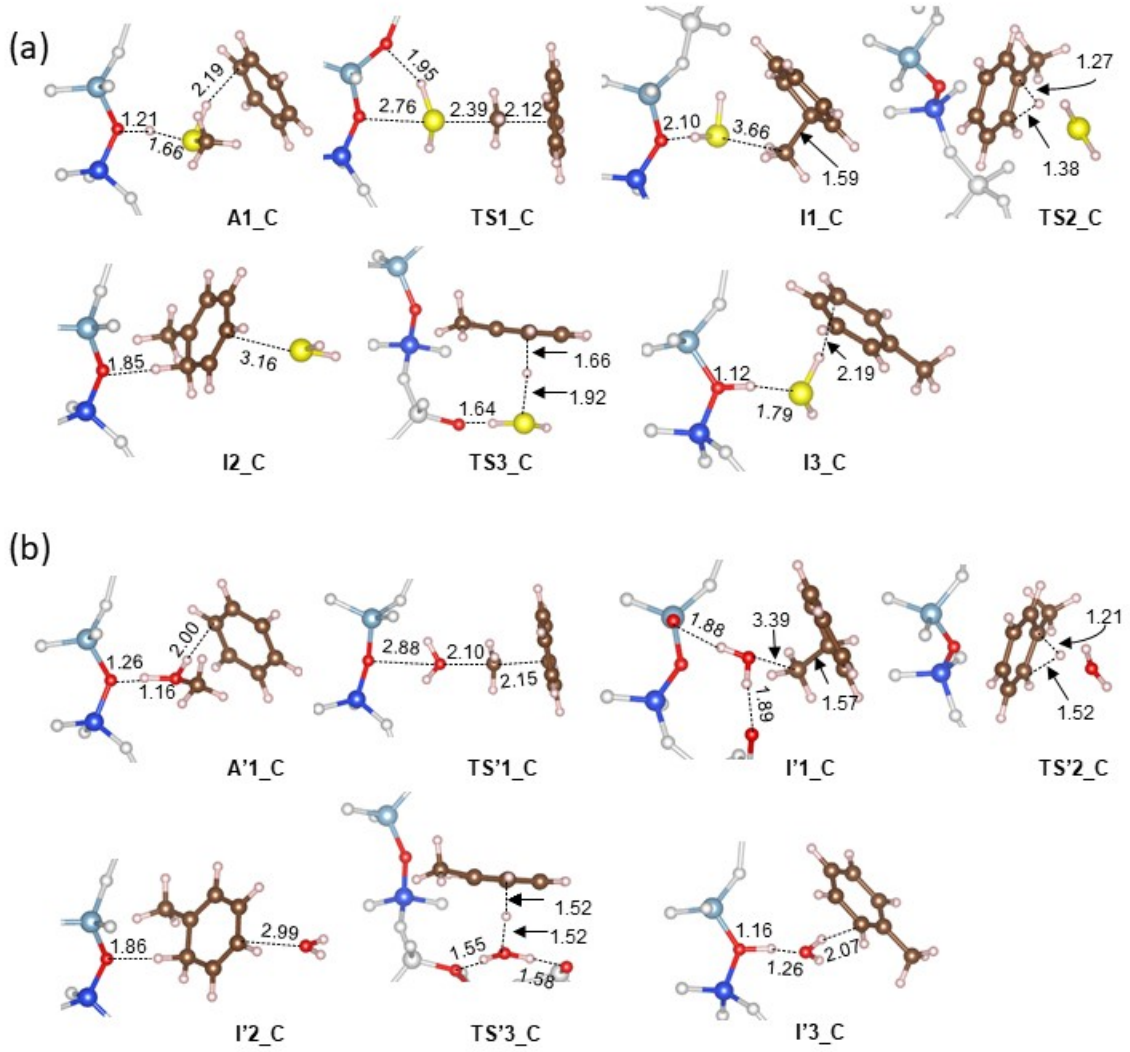

Figure 6: Key geometrical parameters of the optimised structures of adsorbate states (A1_C and A'1_C), transition states (TS1_C, TS'1_C, TS2_C, TS'2_C, TS3_C, TS'3_C) and intermediates (I1_C, I'1_C, I2_C, I'2_C, I3_C, I'3_C) in the concerted mechanism of benzene methylation by mercaptan (a) and by methanol (b) on the free energy surfaces, depicted in Fig. 5. The distances are given in Å and the color code used for the atoms is the following: Si: dark blue, Al: light blue, O: red, C: brown, S: yellow, H: pink. The atoms coloured in light grey correspond to the atoms of the zeolite.

the previous theoretical studies on methanol catalytic methylation over acidic zeolites.[31,64,65] In the case of CH_3OH reagent, the energy barrier (TS'1_C in Fig. 5) to the formation of the C-C bond is commensurable with ΔG_{TS} to methoxy reaction (TS'1 in Fig. 2). In the case of CH_3SH, it requires nearly two times more energy to methylate benzene than in the step-wise

mechanism. In order to unravel the underlying reasons for the significant destabilisation of the TS1_C activation complex we inspected closer its geometrical structure. An elongation of S-H bonds in SH_2 moiety to 1.43 and 1.45 Å is found, whereas in the TS'1_C state the H_2O group remains intact with H-O distances of 1 Å (see Fig. S8(a)). For comparison, the H_2S...CH_3 activation complex (TS1_C in Fig. 3 and Fig. S8(b)) in the mercaptane to methoxy conversion reaction features S-H distances of 1.39 Å and in an isolated H_2S molecules the S-H separation is 1.34 Å. The larger S-H separation in the $C_6H_6 \cdots CH_3 \cdots SH_2$ activation complex is provoked by the presence of benzene in the pores that displaces the mercaptan close to the zeolite pore walls. Consequently, the zeolite oxygens attract the hydrogen atoms in H_2S, causing partial S-H dissociation and a loss of energetic stability of the $C_6H_6 \cdots CH_3 \cdots SH_2$ activation complex. Other possible TS1_C structures have been searched as well by reorienting the CH_3 in TS1_C with one H pointing to the center of benzene ring, as shown in Fig. S8 (c). The converged transition state structure with this orientation was found higher in energy. Other possible transition state configurations were not observed during the 20 ps trajectories from the BOMD simulations starting either with A1_C or TS1_C geometries.

Similar to the toluene formation in the step-wise route, the BOMD simulations revealed a hydrogen transfer first within the toluenium ion, giving rise to a more stable intermediate state I2_C and I'2_C (see Fig. 5 and Fig. 6 for their geometrical structures). This intramolecular H-transfer is also found to be an endothermic process with $\Delta G_{TS} = 26.8$ kcal/mol for mercaptan reagent and $\Delta G_{TS} = 17.1$ kcal/mol for methanol reagent at T=673 K (Table 2). The hydrogen back-donation to the zeolite is mediated by H_2S and H_2O molecules, respectively, overcoming an energy barrier of 45.2 kcal/mol and 32.3 kcal/mol (T = 673 K). Although ΔG_{TS} values of optimized structures at the stationary energy points reveal relatively high energy barriers (especially for mercaptan reagent) the H-transfer is a rapid event at the reactive temperatures according to the short life-time in the order of a few picoseconds for I2 and I3 intermediates. The evolution with time of the characteristic distances to

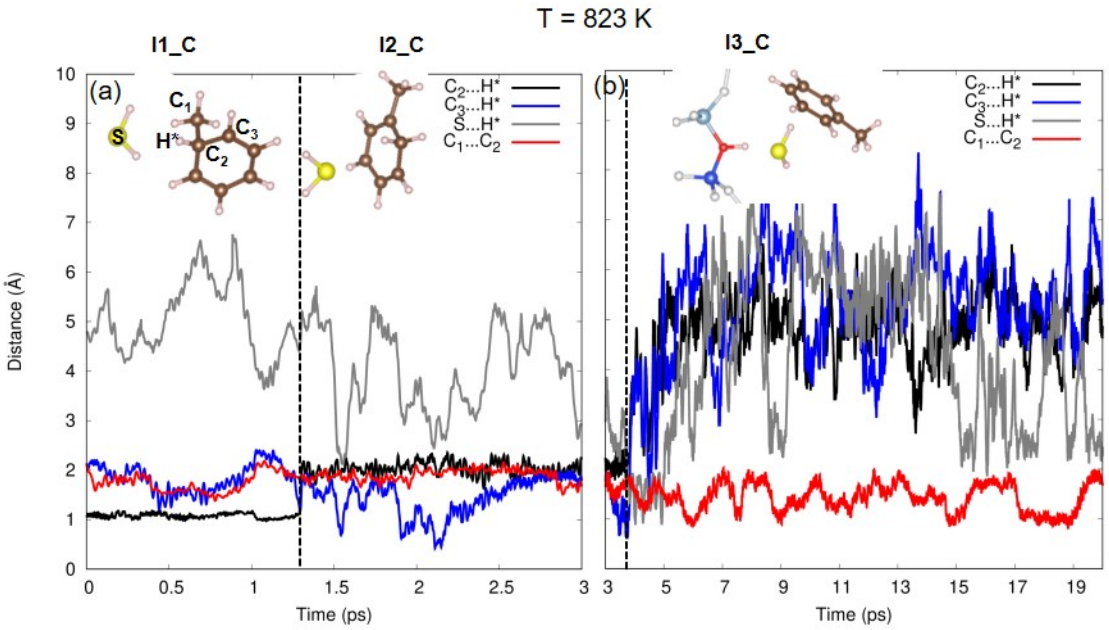

Figure 7: Time evolution of selected C-C and C-H distances in toluenium ion at T = 823 K to show (a) the H^* intramolecular transfer and (b) the deprotonation of $C_7H_9^+$). The color code used for the atoms is: Si: dark blue, Al: light blue, O: red, C: brown, H: light pink.

evidence the H-transfer processes are plotted in Fig. 7, for mercaptan methylation.

Conclusion

The capacity of methyl mercaptan to methylate benzene over H-CHA zeolite catalyst was investigated with DFT (PBE-D3) approach by assuming the step-wise and concerted mechanisms, accepted to be the two fundamental pathways for the methylation of benzene by methanol. For comparison, methanol methylation of benzene was investigated at the same theoretical basis. The basis-set-superposition errors were computed with the counter-poise method and all energies are BSSE corrected. The energy barrier in the rate-limiting reaction to the formation of surface-methoxy from CH_3SH in the step-wise route is higher by 4 kcal/mol than ΔG_{TS} in the same reaction with CH_3OH reagent. This is qualitatively in line with the experimental temperature of mercaptan conversion, established to be higher than the reactive temperature of methanol conversion over H-ZSM-5 zeolite catalysts.[4,5]

The free-energy surface in the concerted mechanism revealed that benzene methylation by mercaptan is unlikely to proceed through this pathway. The rate-limiting reaction in the concerted mechanism, i.e. the formation of C-C bond from the co-adsorbed CH_3SH and C_6H_6, proceeds with an energy barrier that is nearly two-times higher than the activation energy in the step-wise mechanism. This result is attributed to a stronger attraction of H_2S moiety by the zeolite pores when co-adsorbed with benzene causing a partial H-S dissociation. This is the main difference with the methanol reagent, whose conversion over H-CHA catalyst to toluene is found possible along both mechanisms, featuring similar energy barriers in the respective rate-limiting steps. The smaller and less-polarizable H_2O moiety in the $C_6H_6 \cdots CH_3 \cdots H_2O$ activation complex remains intact in the concerted route.

The molecular dynamics simulations, coupled to DFT potential energy surface calculations in the BOMD approach, evidenced rapid intramolecular hydrogen transfers in the toluenium ion to a more-stable intermediate in the step-wise and concerted routes for both CH_3XH (X= O, S) reagents. Moreover, in the concerted route, the hydrogen back-donation to regenerate the H-CHA catalyst is mediated by H_2X molecule. New intermediates and transition states of these intra- and intermolecular H-transfer reactions were consequently identified and considered in the both reaction mechanisms.

Acknowledgement

This work was performed using the HPC resources of CCRT/CINES/IDRIS under the allocation A130807369 by GENCI. Financial support from ECOS project 321168 is gratefully acknowledged.

Supporting Information Available

Supporting figures: PES obtained with pob-DZVP and pob-TZVP basis sets; PES and FES obtained with pob-DZVP and the following exchange-correlation functionals: PBE, B3LYP

and M06 augmented with D3; AIMD temperature fluctuations; key geometrical parameters of the stationary states on FES in the reactions of DMS and DMS formation; geometrical parameters of interest in the co-adsorbed CH_3XH and C_6H_6 structures. Supporting tables: imaginary vibrational frequencies; energies of stationary states at FESs. The fractional coordinates of all states and input file are available in a separated supporting file.

References

(1) Huguet, E.; Coq, B.; Durand, R.; Leroi, C.; Cadours, R.; Hulea, V. A highly efficient process for transforming methyl mercaptan into hydrocarbons and H2S on solid acid catalysts. *Applied Catalysis B: Environmental* **2013**, *134-135*, 344–348.

(2) He, D.; Chen, D.; Hao, H.; Yu, J.; Liu, J.; Lu, J.; Wan, G.; He, S.; Li, K.; Luo, Y. Enhanced activity and stability of Sm-doped HZSM-5 zeolite catalysts for catalytic methyl mercaptan (CH3SH) decomposition. *Chemical Engineering Journal* **2017**, *317*, 60–69.

(3) He, D.; Zhao, Y.; Yang, S.; Mei, Y.; Yu, J.; Liu, J.; Chen, D.; He, S.; Luo, Y. Enhancement of catalytic performance and resistance to carbonaceous deposit of lanthanum (La) doped HZSM-5 catalysts for decomposition of methyl mercaptan. *Chemical Engineering Journal* **2018**, *336*, 579–586.

(4) Cammarano, C.; Gay, E.; Finiels, A.; Fajula, F.; Hulea, V. Toluene Methylation by Methyl Mercaptan and Methanol over Zeolites—A Comparative Study. *ACS Catalysis* **2019**, *9*, 605–609.

(5) Hulea, V.; Huguet, E.; Cammarano, C.; Lacarriere, A.; Durand, R.; Leroi, C.; Cadours, R.; Coq, B. Conversion of methyl mercaptan and methanol to hydrocarbons over solid acid catalysts – A comparative study. *Applied Catalysis B: Environmental* **2014**, *144*, 547–553.

(6) Mashkina, A.; Paukshtis, E.; Krivoruchko, O.; Khairulina, L. N. Conversion of dimethyl disulfide in the presence of zeolites. *Kinet Catal* **2008**, *49*, 253–260.

(7) Tian, P.; Wei, Y.; Ye, M.; Liu, Z. Methanol to Olefins (MTO): From Fundamentals to Commercialization. *ACS Catalysis* **2015**, *5*, 1922–1938.

(8) Olsbye, U.; Svelle, S.; Lillerud, K.; Wei, Z.; Chen, Y.; Li, J.; Wang, J.; Fan, W. The formation and degradation of active species during methanol conversion over protonated zeotype catalysts. *Chemical Society Reviews* **2015**, *44*, 7155–7176.

(9) Haw, J. F.; Song, W.; Marcus, D. M.; Nicholas, J. B. The Mechanism of Methanol to Hydrocarbon Catalysis. *Accounts of Chemical Research* **2003**, *36*, 317–326.

(10) Stöcker, M. Methanol-to-hydrocarbons: catalytic materials and their behavior. *Microporous and mesoporous materials* **1999**, *29*, 3–48.

(11) Ilias, S.; Bhan, A. Mechanism of the catalytic conversion of methanol to hydrocarbons. *Acs Catalysis* **2013**, *3*, 18–31.

(12) Dahl, I. M.; Kolboe, S. On the reaction mechanism for propene formation in the MTO reaction over SAPO-34. *Catalysis Letters* **1993**, *20*, 329–336.

(13) Svelle, S.; Joensen, F.; Nerlov, J.; Olsbye, U.; Lillerud, K.-P.; Kolboe, S.; Bjørgen, M. Conversion of Methanol into Hydrocarbons over Zeolite H-ZSM-5: Ethene Formation Is Mechanistically Separated from the Formation of Higher Alkenes. *Journal of the American Chemical Society* **2006**, *128*, 14770–14771.

(14) Reina, M.; Martinez, A.; Cammarano, C.; Leroi, C.; Hulea, V.; Mineva, T. Conversion of Methyl Mercaptan to Hydrocarbons over H-ZSM-5 Zeolite: DFT/BOMD Study. *ACS Omega* **2017**, *2*, 4647–4656.

(15) Baltrusaitis, J.; Bucko, T.; Michaels, W.; Makkee, M.; Mul, G. Catalytic methyl mercaptan coupling to ethylene in chabazite: DFT study of the first C-C bond formation. *Applied catalysis B: environmental* **2016**, *187*, 195–203.

(16) Wang, S.; Qin, Z.; Dong, M.; Wang, J.; Fan, W. Recent progress on MTO reaction mechanisms and regulation of acid site distribution in the zeolite framework. *Chem Catalysis* **2022**, *2*, 1657–1685.

(17) Liang, T.; Chen, J.; Qin, Z.; Wang, S.; Wang, P.; Jin, F.; Dong, M.; Wang, J.; Fan, W. Insight into induction period of methanol conversion reaction: Reactivity of ethene-precursors over H-ZSM-5 zeolite is independent of Brønsted acid site density. *Fuel* **2023**, *332*, 126062.

(18) Fan, S.; Wang, H.; He, S.; Yuan, K.; Wang, P.; Li, J.; Wang, S.; Qin, Z.; Dong, M.; Fan, W. et al. Formation and evolution of methylcyclohexene in the initial period of methanol to olefins over H-ZSM-5. *ACS Catalysis* **2022**, *12*, 12477–12487.

(19) Ren, L.; Wang, B.; Lu, K.; Peng, R.; Guan, Y.; Jiang, J.-g.; Xu, H.; Wu, P. Selective conversion of methanol to propylene over highly dealuminated mordenite: Al location and crystal morphology effects. *Chinese Journal of Catalysis* **2021**, *42*, 1147–1159.

(20) Botchway, C. H.; Tia, R.; Adei, E.; O'malley, A. J.; Dzade, N. Y.; Hernandez-Tamargo, C.; de Leeuw, N. H. Influence of topology and Brønsted acid site presence on methanol diffusion in zeolites beta and MFI. *Catalysts* **2020**, *10*, 1342.

(21) Forester, T.; Howe, R. F. In situ FTIR studies of methanol and dimethyl ether in ZSM-5. *Journal of the American Chemical Society* **1987**, *109*, 5076–5082.

(22) Cheung, P.; Bhan, A.; Sunley, G. J.; Law, D. J.; Iglesia, E. Site requirements and elementary steps in dimethyl ether carbonylation catalyzed by acidic zeolites. *Journal of Catalysis* **2007**, *245*, 110–123.

(23) Yamazaki, H.; Shima, H.; Imai, H.; Yokoi, T.; Tatsumi, T.; Kondo, J. N. Evidence for a "Carbene-like" Intermediate during the Reaction of Methoxy Species with Light Alkenes on H-ZSM-5. *Angewandte Chemie International Edition* **2011**, *50*, 1853–1856.

(24) Song, W.; Haw, J. F.; Nicholas, J. B.; Heneghan, C. S. Methylbenzenes are the organic reaction centers for methanol-to-olefin catalysis on HSAPO-34. *Journal of the American Chemical Society* **2000**, *122*, 10726–10727.

(25) Bosacek, V. Formation of surface-bonded methoxy groups in the sorption of methanol and methyl iodide on zeolites studied by carbon-13 MAS NMR spectroscopy. *The Journal of Physical Chemistry* **1993**, *97*, 10732–10737.

(26) Wang, W.; Buchholz, A.; Seiler, M.; Hunger, M. Evidence for an initiation of the methanol-to-olefin process by reactive surface methoxy groups on acidic zeolite catalysts. *Journal of the American Chemical Society* **2003**, *125*, 15260–15267.

(27) Wang, W.; Hunger, M. Reactivity of surface alkoxy species on acidic zeolite catalysts. *Accounts of chemical research* **2008**, *41*, 895–904.

(28) Jiang, Y.; Hunger, M.; Wang, W. On the reactivity of surface methoxy species in acidic zeolites. *Journal of the American Chemical Society* **2006**, *128*, 11679–11692.

(29) Mirth, G.; Lercher, J. A. Coadsorption of toluene and methanol on HZSM-5 zeolites. *The Journal of Physical Chemistry* **1991**, *95*, 3736–3740.

(30) Brogaard, R. Y.; Henry, R.; Schuurman, Y.; Medford, A. J.; Moses, P. G.; Beato, P.; Svelle, S.; Nørskov, J. K.; Olsbye, U. Methanol-to-hydrocarbons conversion: The alkene methylation pathway. *Journal of catalysis* **2014**, *314*, 159–169.

(31) Odedairo, T.; Al-Khattaf, S. Comparative study of zeolite catalyzed alkylation of benzene with alcohols of different chain length: H-ZSM-5 versus mordenite. *Catalysis today* **2013**, *204*, 73–84.

(32) Xu, S.; Zheng, A.; Wei, Y.; Chen, J.; Li, J.; Chu, Y.; Zhang, M.; Wang, Q.; Zhou, Y.; Wang, J. et al. Direct Observation of Cyclic Carbenium Ions and Their Role in the Catalytic Cycle of the Methanol-to-Olefin Reaction over Chabazite Zeolites. *Angewandte Chemie International Edition* **2013**, *52*, 11564–11568.

(33) Van Speybroeck, V.; Hemelsoet, K.; De Wispelaere, K.; Qian, Q.; Van der Mynsbrugge, J.; De Sterck, B.; Weckhuysen, B. M.; Waroquier, M. Mechanistic Studies on Chabazite-Type Methanol-to-Olefin Catalysts: Insights from Time-Resolved UV/Vis Microspectroscopy Combined with Theoretical Simulations. *ChemCatChem* **2013**, *5*, 173–184.

(34) Ferri, P.; Li, C.; Millán, R.; Martínez-Triguero, J.; Moliner, M.; Boronat, M.; Corma, A. Impact of Zeolite Framework Composition and Flexibility on Methanol-To-Olefins Selectivity: Confinement or Diffusion? *Angewandte Chemie International Edition* **2020**, *59*, 19708–19715.

(35) Dovesi, R.; Erba, A.; Orlando, R.; Zicovich-Wilson, C. M.; Civalleri, B.; Maschio, L.; Rérat, M.; Casassa, S.; Baima, J.; Salustro, S. et al. Quantum-mechanical condensed matter simulations with CRYSTAL. *Wiley Interdisciplinary Reviews: Computational Molecular Science* **2018**, *8*, e1360.

(36) Fletcher, R. *Practical methods of optimization*; John Wiley & Sons, 2013.

(37) Rimola, A.; Zicovich-Wilson, C. M.; Dovesi, R.; Ugliengo, P. Search and Characterization of Transition State Structures in Crystalline Systems Using Valence Coordinates. *Journal of Chemical Theory and Computation* **2010**, *6*, 1341–1350.

(38) Schlegel, H. B. Geometry optimization. *WIREs Computational Molecular Science* **2011**, *1*, 790–809.

(39) Monkhorst, H. J.; Pack, J. D. Special points for Brillouin-zone integrations. *Phys. Rev. B* **1976**, *13*, 5188–5192.

(40) Pascale, F.; Zicovich-Wilson, C. M.; López Gejo, F.; Civalleri, B.; Orlando, R.; Dovesi, R. The calculation of the vibrational frequencies of crystalline compounds and its implementation in the CRYSTAL code. *Journal of computational chemistry* **2004**, *25*, 888–897.

(41) Zicovich-Wilson, C. M.; Pascale, F.; Roetti, C.; Saunders, V.; Orlando, R.; Dovesi, R. Calculation of the vibration frequencies of α-quartz: The effect of Hamiltonian and basis set. *Journal of computational chemistry* **2004**, *25*, 1873–1881.

(42) Peintinger, M. F.; Oliveira, D. V.; Bredow, T. Consistent Gaussian basis sets of triple-zeta valence with polarization quality for solid-state calculations. *Journal of Computational Chemistry* **2013**, *34*, 451–459.

(43) Román-Román, E. I.; Zicovich-Wilson, C. M. The role of long-range van der Waals forces in the relative stability of SiO2-zeolites. *Chemical Physics Letters* **2015**, *619*, 109–114.

(44) Perdew, J. P.; Burke, K.; Ernzerhof, M. Generalized gradient approximation made simple. *Physical review letters* **1996**, *77*, 3865.

(45) Perdew, J. P.; Burke, K.; Wang, Y. Generalized gradient approximation for the exchange-correlation hole of a many-electron system. *Physical review B* **1996**, *54*, 16533.

(46) Becke, A. D. A new mixing of Hartree–Fock and local density-functional theories. *The Journal of chemical physics* **1993**, *98*, 1372–1377.

(47) Stephens, P. J.; Devlin, F. J.; Chabalowski, C. F.; Frisch, M. J. Ab initio calculation of vibrational absorption and circular dichroism spectra using density functional force fields. *The Journal of physical chemistry* **1994**, *98*, 11623–11627.

(48) Zhao, Y.; Truhlar, D. G. A new local density functional for main-group thermochemistry, transition metal bonding, thermochemical kinetics, and noncovalent interactions. *The Journal of chemical physics* **2006**, *125*, 194101.

(49) Grimme, S.; Antony, J.; Ehrlich, S.; Krieg, H. A consistent and accurate ab initio parametrization of density functional dispersion correction (DFT-D) for the 94 elements H-Pu. *The Journal of chemical physics* **2010**, *132*, 154104.

(50) Grimme, S.; Ehrlich, S.; Goerigk, L. Effect of the damping function in dispersion corrected density functional theory. *Journal of computational chemistry* **2011**, *32*, 1456–1465.

(51) Grimme, S.; Hansen, A.; Brandenburg, J. G.; Bannwarth, C. Dispersion-corrected mean-field electronic structure methods. *Chemical reviews* **2016**, *116*, 5105–5154.

(52) Plessow, P. N.; Studt, F. Unraveling the mechanism of the initiation reaction of the methanol to olefins process using ab initio and DFT calculations. *ACS catalysis* **2017**, *7*, 7987–7994.

(53) Giannozzi, P.; Baroni, S.; Bonini, N.; Calandra, M.; Car, R.; Cavazzoni, C.; Ceresoli, D.; Chiarotti, G. L.; Cococcioni, M.; Dabo, I. et al. QUANTUM ESPRESSO: a modular and open-source software project for quantum simulations of materials. *Journal of physics: Condensed matter* **2009**, *21*, 395502.

(54) Giannozzi, P.; Andreussi, O.; Brumme, T.; Bunau, O.; Nardelli, M. B.; Calandra, M.; Car, R.; Cavazzoni, C.; Ceresoli, D.; Cococcioni, M. et al. Advanced capabilities for materials modelling with Quantum ESPRESSO. *Journal of physics: Condensed matter* **2017**, *29*, 465901.

(55) Quantum Espresso. http://www.quantum-espresso.org/(accessed March 28, 2024).

(56) Quantum Espresso Pseudopotentials. http://www.quantum-espresso.org/pseudopotentials/(accessed March 28, 2024).

(57) Berendsen, H. J.; Postma, J. v.; Van Gunsteren, W. F.; DiNola, A.; Haak, J. R. Molecular dynamics with coupling to an external bath. *The Journal of chemical physics* **1984**, *81*, 3684–3690.

(58) Lemak, A.; Balabaev, N. On the Berendsen thermostat. *Molecular Simulation* **1994**, *13*, 177–187.

(59) Swope, W. C.; Andersen, H. C.; Berens, P. H.; Wilson, K. R. A computer simulation method for the calculation of equilibrium constants for the formation of physical clusters of molecules: Application to small water clusters. *The Journal of chemical physics* **1982**, *76*, 637–649.

(60) Verlet, L. Computer" experiments" on classical fluids. I. Thermodynamical properties of Lennard-Jones molecules. *Physical review* **1967**, *159*, 98.

(61) Sierka, M.; Sauer, J. Proton mobility in Chabazite, Faujasite, and ZSM-5 Zeolite catalysts. Comparison based on ab initio calculations. *The journal of physical chemistry B* **2001**, *105*, 1603–1613.

(62) Baerlocher, C.; McCusker, L. Database of Zeolite Structures. http://www.iza-structure.org/databases/(accessed March 28, 2024).

(63) Calligaris, M.; Nardin, G.; Randaccio, L. Cation site location in hydrated chabazites. Crystal structure of potassium-and silver-exchanged chabazites. *Zeolites* **1983**, *3*, 205–208.

(64) Wen, Z.; Zhu, H.; Zhu, X. Density functional theory study of the zeolite-catalyzed methylation of benzene with methanol. *Catalysis Letters* **2020**, *150*, 21–30.

(65) Wen, Z.; Yang, D.; He, X.; Li, Y.; Zhu, X. Methylation of benzene with methanol over HZSM-11 and HZSM-5: A density functional theory study. *Journal of Molecular Catalysis A: Chemical* **2016**, *424*, 351–357.

(66) Van der Mynsbrugge, J.; Visur, M.; Olsbye, U.; Beato, P.; Bjørgen, M.; Van Speybroeck, V.; Svelle, S. Methylation of benzene by methanol: Single-site kinetics over H-ZSM-5 and H-beta zeolite catalysts. *Journal of Catalysis* **2012**, *292*, 201–212.

(67) Vigné-Maeder, F.; Jobic, H. Adsorption sites and packing of benzene in silicalite. *Chemical Physics Letters* **1990**, *169*, 31–35.

(68) Chang, C. D.; Silvestri, A. J. The conversion of methanol and other O-compounds to hydrocarbons over zeolite catalysts. *Journal of Catalysis* **1977**, *47*, 249–259.

(69) Jones, A. J.; Iglesia, E. Kinetic, spectroscopic, and theoretical assessment of associative and dissociative methanol dehydration routes in zeolites. *Angewandte Chemie* **2014**, *126*, 12373–12377.

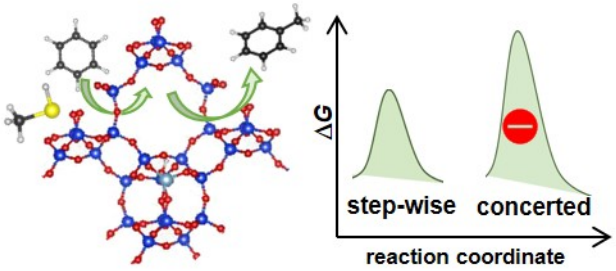

TOC Graphic